Substituent Effects on Oxidative Addition for Coordinatively Unsaturated d^8 ML_3. Mechanistic and Thermodynamic Considerations

Ming-Der Su* and San-Yan Chu*

Department of Chemistry, National Tsing Hua University, Hsinchu 30043, Taiwan, R.O.C

Received: July 2, 1998

A density functional theory study has been carried out for oxidative addition of the H−CH_3 bond to coordinatively unsaturated 14-electron T-shaped M(L_n)(L'_{3-n}) complexes, where M = Ru or Os, and L and L′ = PH_3 or CO. All the stationary points were determined at the B3LYP/LANL2DZ level of theory. It has been found that there should be two competing pathways in those reactions, which can be classified as a σ or π approach. The former was proved to be more favorable with a very low activation energy. A configuration mixing model has been used to develop an explanation for the origin of the barrier heights as well as the reaction enthalpies. Considering the substituent effect and the nature of the metal center, the following conclusions therefore emerge: for a 14-electron T-shaped *trans*-M(L″)L_2 complex (L″ = ligand trans to the incoming methane), a better electron-donating ligand L″ (such as PH_3 and Cl) with a heavier transition-metal center (third-row) will be a potential model for the oxidative addition of saturated C−H bonds. In addition, transition-metal fragment ML_3 containing more electron-releasing alkylphosphines ligands can facilitate the oxidative addition.

I. Introduction

The carbon−hydrogen bond activations of alkanes brought about by transition-metal complexes are of fundamental interest in various areas of chemical research, such as organometallic chemistry, biochemistry, organic chemistry, and, most importantly, catalytic research.[1] Unsurprisingly, the importance of this reaction has resulted in the accumulation of a large body of experimental and theoretical results.[2,3] Nevertheless, mechanistic studies of carbon−hydrogen bond activation reactions have been difficult because of low quantum yields, which make it impossible to observe reactive intermediates.[2] Theory is therefore a potentially useful partner to experiment in the investigation of the mechanism of the oxidative additions of C−H bonds.

A decade ago, Flood and co-workers reported that the thermolysis of *cis*-$L_4Os(H)(CH_2CMe_3)$ (L = $P(CH_3)_3$) in methane at 80 °C results in the formation of $L_3Os(H)(CH_3)$, which was recognized as one of the first observations of a non-cyclopentadienyl-containing methyl hydride complex from reaction of a soluble complex with methane.[4] This aroused our interest to investigate the potential energy surfaces of such reactions using the density functional theory (DFT).[5] A study of the important C−H activation reaction, eq 1, was thus undertaken.

$$M(L_n)(L'_{3-n}) + H-CH_3 \rightarrow M(L_n)(L'_{3-n})(H)(CH_3) \quad (1)$$

For the present, the focus is on C−H activation by 14-electron complexes of the form M(L_n)(L'_{3-n}), where M = Ru or Os, and L and L′ = PH_3 or CO.[6]

The reasons for choosing eq 1 as the model are the following. (i) Many theoretical studies have been performed on a C−H oxidative addition to Rh, Ir, Pd, and Pt organometallic species.[1k,l,s,3,5] However, only a few have actually been carried out on oxidative additions by other transition-metal complexes. Very little is known on how much the C−H oxidative addition is influenced by Ru and Os metals and ancillary ligands. (ii) Although much work has been done by organic researchers regarding substituent effects on the rates and mechanisms of organic reactions, few studies of this type have been attempted for organometallic systems. Additionally, to our knowledge, there are no systematic theoretical calculations for the substituent effect on the 14-electron d^8 ML_3 systems. Through this theoretical study, we hope (a) to obtain a detailed understanding of the C−H oxidative addition to 14-electron d^8 ML_3 type complexes, (b) to investigate the influence of different ligands upon the geometries and energies of the intermediates, as well as the transition states, (c) to elucidate the differences between Ru and Os, (d) to probe electronic effects on the reactivities in numerous variations in the metals and ligands, and (e) to bring out the determined factor that controls the activation barrier for oxidative reactions. It is our intention to show clearly that the singlet−triplet gap of the 14-electron d^8 ML_3 species can be a guide to predict its reactivity for oxidative addition reactions.

The order of this paper is as follows. After the Introduction and the electronic structures of the model systems, we present in the third and fourth sections the calculational results of eq 1 for Ru and Os, respectively. The origin of the barrier heights and reaction enthalpies for oxidative addition of coordinatively unsaturated transition-metal complexes is discussed in section V. Section VI contains brief concluding remarks. Details of the calculations are given in the Appendix.

II. Electronic Structure of ML_3 + CH_4

Before discussing the geometrical optimizations and the potential energy surfaces for oxidative additions, we shall discuss the bonding in the complex. From this, one may then build a frontier molecular orbital (FMO) model on the basis of a set of fragment MOs. This has been proven to be a good approach that allows one to predict the approximate reaction trajectory and transition-state structure for the insertion of the

10.1021/jp982861o CCC: $15.00
Published on Web 11/13/1998

CHART 1

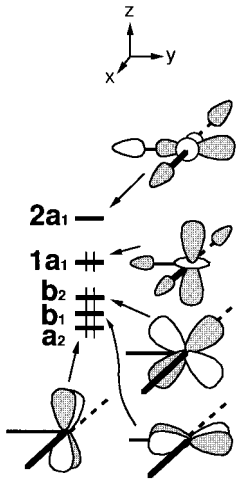

carbene-like species into the saturated C−H bonds.[7] Note that this concept for the insertion mechanism was expressed for the first time by Bach. In this work, we shall therefore use the FMO model to search for the transition states of the oxidative addition reaction of the 14-electron ML_3 complex that is isolobal to methylene.[8]

It is convenient to divide the reactants into d^8 C_{2v} ML_3 and CH_4 fragments and to begin a discussion of the bonding by looking briefly at the valence orbitals of the ML_3 and CH_4 units. The orbitals of a d^8 C_{2v} ML_3 fragment, displayed in Chart 1, have been extensively discussed elsewhere.[9,10] At low energy are three closely spaced levels $1b_1(d_{xy})$, $1a_2(d_{xz})$, and $1b_2(d_{yz})$, which are essentially pure metal d orbitals. The occupied $1a_1$ orbital, which consists primarily of metal d_{z^2} orbital, lies somewhat higher in energy than the others because it is destabilized by the ligand σ orbitals. At higher energy is an empty orbital termed $2a_1$, which is primarily $d_{x^2-y^2}$. Furthermore, metal p_y and s characteristics are mixed into it. This hybridization is done so that the orbital is directed away from the three ligands toward the empty coordinate site. Those fragment orbitals in Chart 1 are appropriate for any ligand set of σ donors. Nevertheless, π effects can be introduced to influence the ordering of levels for the d^8 C_{2v} ML_3 fragment, thus allowing various configurations to be made (vide infra).

Since a d^8 C_{2v} ML_3 fragment is isolobal with CH_2, then each should have two valence orbitals with the same symmetry properties.[8] These are shown in **1**, in which each fragment has

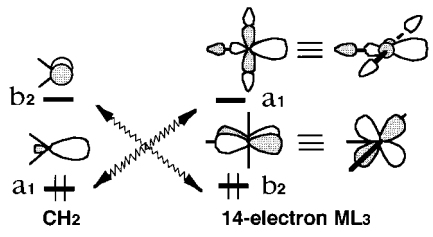

1

one orbital of a_1 and b_2 symmetry. Note that the ordering of the two orbitals a_1 and b_2 differs for CH_2 and ML_3. This is a natural consequence of the fact that in ML_3 the major contribution to the b_2 orbital is the metal d character, while in the a_1 orbital, it is a hybrid of metal s, p, and d characteristics, as mentioned earlier. Therefore, for a singlet CH_2 fragment one would assign the two electrons to the a_1 orbital, while for a singlet 14-electron T-shaped ML_3, the two electrons would go into the b_2 level.

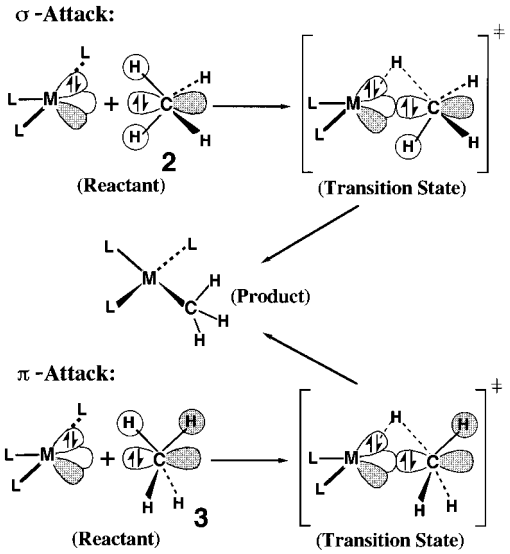

Figure 1. Insertion of 14-electron ML_3 into hydrocarbons can proceed along a σ_{CH_2} path, where the empty ML_3 s/p/d orbital is aligned with the carbon p orbital of a σ_{CH_2} fragment orbital, or along a π_{CH_2} path, where the ML_3 orbital is aligned with a π_{CH_2} fragment orbital.

On the other hand, in a canonical MO description of a hydrocarbon, there are no isolated MOs that describe a particular C−H σ bond. For instance, in methane there is a lower lying $2A_1$ orbital and three degenerate T_2 orbitals.[11] In a tetrahedral array, both hydrogens directly bound to the sp^3 carbon occupy a common plane, and they are related by symmetry and may comprise an orbital with σ or π symmetry as in **2** (σ_{CH2}) and **3** (π_{CH2}), respectively.[12]

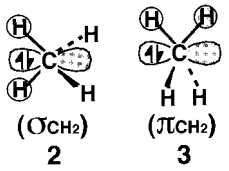

From the above discussion, it is clear that the main relevant orbitals on the metal center of the d^8 C_{2v} ML_3 fragment are the empty hybrid orbital (i.e., a_1 as shown in **1**), pointing toward the vacant site of ML_3, and the filled b_2 orbital, which interact with a hydrocarbon fragment orbital, as given in **2** or **3**, to serve as the terminus for a concerted 1,2-hydrogen migration. As seen in Figure 1, the FMO model therefore suggests that the starting geometry of 14-electron T-shaped ML_3 may approach methane from two unique directions. One is the σ attack. That is, the empty a_1 orbital of ML_3 overlaps with a σ_{CH_2} hydrocarbon orbital along the axis of its filled atomic p orbital and a 1,2-hydrogen migration to the adjacent pair of electrons (b_2) takes place in concert with metal−carbon bond formation. The other is the π attack, which proceeds by attack of a filled π_{CH_2} hydrocarbon orbital along the axis of the empty a_1 metal orbital with a concerted hydrogen migration to the ML_3 lone pair (b_2). Both of these attacks are stabilizing because of the two-electron interactions,[7] and they entail the same important results: the formation of a new metal−carbon σ bond as well as a new metal−hydrogen σ bond, accompanied by the breaking of the C−H σ bond. This is a typical example of the oxidative addition reaction of a transition-metal complex into the C−H bond.[1] We shall see the calculational results supporting these predictions below.

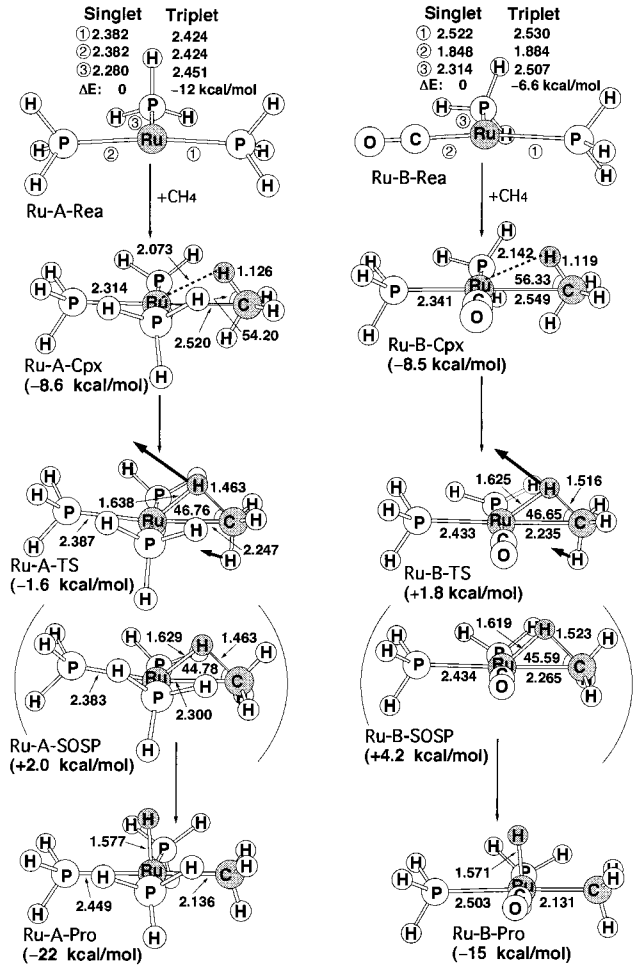

Figure 2. B3LYP/LANL2DZ optimized geometries (in angstroms and degrees) of the reactants (singlet and triplet), precursor complex, transition state, and product of Ru−**A** and Ru−**B** cases. Values in parentheses are the relative energies at the B3LYP/LANL2DZ level. The heavy arrows indicate the main atomic motions in the transition-state eigenvector.

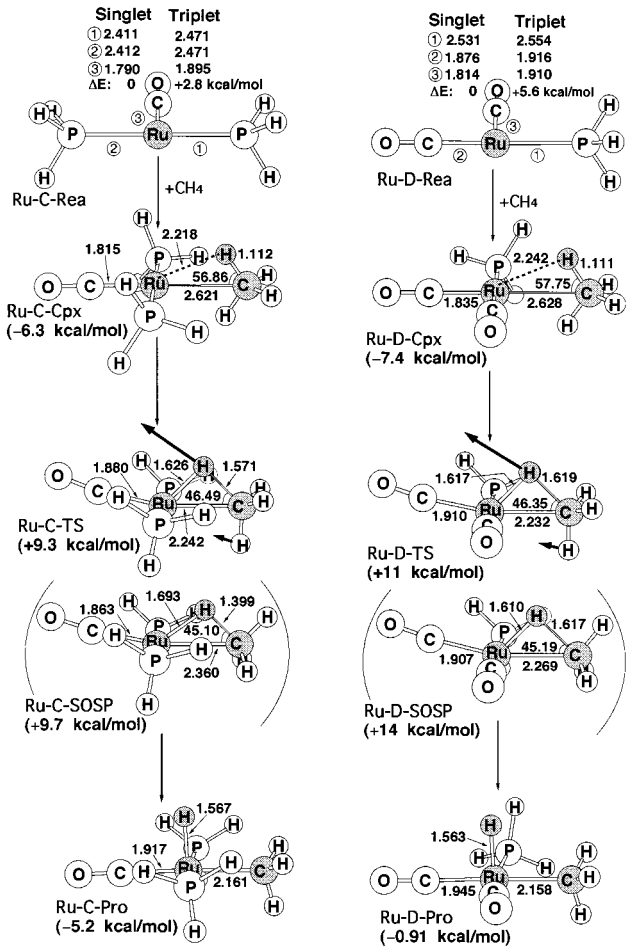

Figure 3. B3LYP/LANL2DZ optimized geometries (in angstroms and degrees) of the reactants (singlet and triplet), precursor complex, transition state, and product of Ru−**C** and Ru−**D** cases. Values in parentheses are the relative energies at the B3LYP/LANL2DZ level. The heavy arrows indicate the main atomic motions in the transition-state eigenvector.

The six sets of reactants used in the present work are shown in **4** with M = Ru, Os: **A** (all ligands cis), **B** (two PH_3 ligands

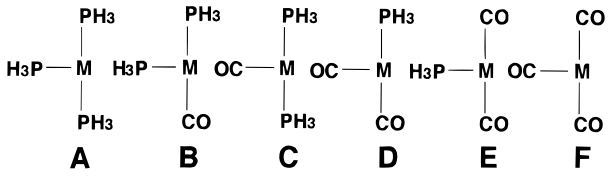

4

cis), **C** (two PH_3 ligands trans), **D** (two CO ligands cis), **E** (two CO ligands trans), and **F** (all ligands cis).

III. Geometries and Energetics of $RuL_3 + CH_4$

In this section the results for four regions on the potential energy surfaces will be presented: 14-electron $Ru(L_n)(L'_{3-n})$ plus free CH_4 (Rea), a precursor complex (Cpx), the transition state (TS), and the oxidative addition product (Pro) $Ru(L_n)(L'_{3-n})(H)(CH_3)$. The fully optimized geometries for those stationary points calculated at the B3LYP/LANL2DZ level are given in Figures 2−4, respectively. Total and relative energies are collected in Table 1.

Several interesting conclusions can be drawn from these figures and the table. First, compounds Ru−**A**−Rea−Ru−**F**−Rea have been calculated both as low-spin (singlet) and as high-spin (triplet state) complexes. It turns out that the complexes Ru−**A**−Rea, Ru−**B**−Rea, and Ru−**E**−Rea, with a PH_3 ligand occupying the equatorial position, possess a triplet ground state, whereas the other complexes, having a CO ligand in the equatorial site, prefer the singlet ground state. This is because the accessibility of an electron-donating σ orbital on the PH_3 group is responsible for the decrease in energy of the $2a_1$ orbital (see Chart 1).[13] Additionally, this σ-donor ligand also pushes the $1a_1$ up in energy.[14] Thus, these two effects will lead to a smaller HOMO($1a_1$)−LUMO($2a_1$) energy difference. In contrast, a π-acceptor ligand such as CO will stabilize the b_2 and a_2 orbitals and then lower their energies , while the energies of other orbitals are kept relatively constant. Consequently, the open-shell triplet state is of lowest energy for the complexes Ru−**A**−Rea, Ru−**B**−Rea, and Ru−**E**−Rea, whereas the closed-shell singlet state is of lowest energy for the complexes Ru−**C**−Rea, Ru−**D**−Rea, and Ru−**F**−Rea.

Second, in the triplet state of a 14-electron, T-shaped ML_3, one electron is situated in the $2a_1$ orbital, in which antibonding interactions exist between the metal and the three ancillary ligands, whereas this orbital is empty in the singlet state. The distance r(M−L) between the metal atom and the ligand, L, is therefore expected to be larger for the triplet compared to the singlet. This prediction qualitatively agrees with our B3LYP/LANL2DZ results for all cases as given in Figures 2−4.

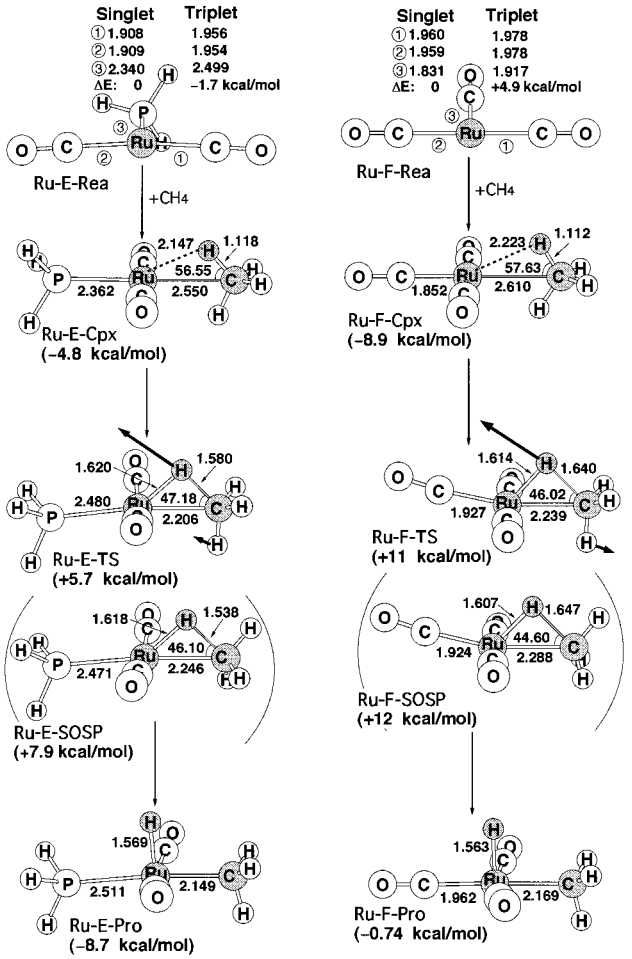

Figure 4. B3LYP/LANL2DZ optimized geometries (in angstroms and degrees) of the reactants (singlet and triplet), precursor complex, transition state, and product of Ru−**E** and Ru−**F** cases. Values in parentheses are the relative energies at the B3LYP/LANL2DZ level. The heavy arrows indicate the main atomic motions in the transition-state eigenvector.

TABLE 1: Relative Energies for Singlet and Triplet ML_3 Fragments and for the Process $ML_3 + H-CH_3 \rightarrow$ Precursor Complex → Transition State → Product[a]

system	singlet, kcal/mol	ΔE_{st},[b] kcal/mol	reactant, kcal/mol	ΔE_{int},[c] kcal/mol	ΔE_{act},[d] kcal/mol	ΔH,[e] kcal/mol
Ru−**A**	0	−11.8	0	−8.64	−1.57	−21.8
Ru−**B**	0	−6.58	0	−8.54	+1.79	−14.8
Ru−**C**	0	+2.81	0	−6.30	+9.32	−5.17
Ru−**D**	0	+5.56	0	−7.41	+11.3	−0.912
Ru−**E**	0	−1.70	0	−4.83	+5.68	−8.55
Ru−**F**	0	+4.86	0	−8.94	+10.9	−0.744
Os−**A**	0	−3.91	0	−7.01	−6.14	−38.9
Os−**B**	0	−2.97	0	−9.33	−5.54	−35.0
Os−**C**	0	+8.51	0	−5.52	+0.398	−24.8
Os−**D**	0	+8.31	0	−8.38	+1.82	−21.0
Os−**E**	0	+0.590	0	−11.2	−3.73	−26.8
Os−**F**	0	+4.71	0	−10.8	+2.20	−21.0

[a] At the B3LYP/LANL2DZ level. [b] Energy relative to the corresponding singlet state. A negative value means the triplet is the ground state. [c] The stabilization energy of the precursor complex relative to the corresponding reactants. [d] The activation energy of the transition state relative to the corresponding reactants. [e] The exothermicity of the product relative to the corresponding reactants.

Additionally, the DFT results also indicate that the Ru−**C**−Rea complex is 9.4 kcal/mol more stable than the Ru−**B**−Rea isomer in the singlet state. Likewise, the singlet Ru−**D**−Rea complex is 10 kcal/mol lower in energy than the singlet Ru−**E**−Rea isomer. The electronic preference for Ru−**C**−Rea and Ru−**D**−Rea can be explained by the relative strength of CO and PH_3 as trans-destabilizing ligands with CO > PH_3.[15]

Third, since the DFT calculations suggest that the complexes Ru−**A**−Rea, Ru−**B**−Rea, and Ru−**E**−Rea should adopt a triplet ground state, this implies that those complexes might insert into the saturated C−H bond via a diradical-type mechanism. Nevertheless, it is well established that whenever a reactant contains a heavy atom center, which is not necessarily directly involved in the reaction, a strong spin−orbit coupling (SOC) may occur.[16] In other words, a triplet reactant, via the agency of the heavy atom, can undergo a spin-inversion process for transformation to the singlet reactant and then proceed along the singlet reaction. In addition, our DFT results in Table 1 also suggested that those reactants with the triplet ground state would have a small excitation energy to the first singlet state; i.e., $\Delta E_{st} = -12 - -1.7$ kcal/mol. Thus, owing to the fact that RuL_3 has a small singlet−triplet splitting ΔE_{st} and that a heavier transition metal is involved, the SOC is expected to be substantial in those oxidative additions and would wash out differentials based on singlet and triplet distinctions. For these reasons, it could well be that the oxidative addition reactions proceed on the singlet surface, even if the reactants start from the triplet state. We shall therefore focus on the singlet surface from now on.

Fourth, the precursor complexes (Ru−**A**−Cpx−Ru−**F**−Cpx) all display very similar Ru···(CH_4) bonding characteristics. The methane ligand is coordinated to Ru in an η^3 fashion via two C−H σ bonds with the H−C−H plane nearly orthogonal to the RuL_3 coordination plane and the L″−Ru−CH_4 (L″ = ligand trans to methane) angle close to 180°. In addition, the distance between the carbon and the migrating hydrogen in the methane moiety, for the precursor complexes studied here, is slightly elongated (1.11−1.13 Å), compared to 1.10 Å in free CH_4. The Ru−C distance to CH_4 in the precursor complexes Ru−**A**−Rea, Ru−**B**−Rea, and Ru−**E**−Rea is 2.52, 2.55, and 2.55 Å, respectively, whereas Ru−**C**−Rea, Ru−**D**−Rea, and Ru−**F**−Rea have a Ru−C distance of 2.62, 2.63, and 2.61 Å, respectively. We attribute the weak intermediate bond and long Ru−C distance in the latter three precursor complexes to the stronger trans-destabilizing effect of CO compared to PH_3.

Fifth, as shown in Figures 2−4, the σ_{CH_2} and π_{CH_2} approaches can lead to a transition state (with one imaginary frequency) and a second-order saddle point (with two imaginary frequencies), respectively, as determined by the frequency calculations at the B3LYP/LANL2DZ level. The transition-state vectors represented by the heavy arrows in the complexes Ru−**A**−TS − Ru−**F**−TS all are in accordance with the insertion process, primarily the C−H bond stretching with a hydrogen migrating to the metal center. Examination of the conformations of those saddle points (Ru−**A**−TS−Ru−**F**−TS and Ru−**A**−SOSP−Ru−**F**−SOSP) for each oxidative addition reaction provides excellent confirmation of the earlier prediction where ML_3 attacks the σ_{CH_2} and π_{CH_2} fragment orbitals along the axis of the central metal spd hybrid orbital. It is noted that such characteristic three-center transition states have been observed in oxidative additions of C−H bonds to 16-electron $CpML_2$[17a] and $CpML$[7e] and 14-electron ML_3[5f] and ML_2 systems.[17b,c] Moreover, comparing the σ attack and the π attack in Figure 1, one can readily anticipate that the ML_3 insertion in the σ_{CH_2} orientation has fewer steric interactions than a π_{CH_2} approach because of the steric effect and produces the insertion product in its staggered lower energy conformation. This prediction is confirmed by our calculational results as given in Table 1. For

instance, the activation barrier of the σ_{CH_2} approach is lower in energy than that of the π_{CH_2} insertion by about 3.6−0.37 kcal/mol for the RuL_3 cases at the B3LYP level of theory.

Sixth, as expected in the transition-state structure, the C−H′ (H′ = the migrating hydrogen atom) bond length is generally increased, while the forming Ru−H′ and Ru−C bonds are also quite long. For reactions of CH_4 with Ru−**A**−Rea, Ru−**B**−Rea, and Ru−**E**−Rea, the breaking C−H′ bond lengths are 1.46, 1.52, and 1.58 Å, respectively, while the forming Ru−H′ (Ru−C) bond lengths are 1.64 (2.25), 1.63 (2.24), and 1.62 (2.21) Å. The changes in the C−H′, Ru−H′, and Ru−C bond lengths in the transition structure are more reactant-like for Ru−**A**, Ru−**B**, and Ru−**E** systems, in accordance with the large exothermicity of the oxidative addition process. However, in the case of Ru−**C**, Ru−**D**, and Ru−**F**, the breaking C−H′ bond length (i.e., 1.57, 1.62, and 1.61 Å, respectively) is significantly longer than in the case for Ru−**A**, Ru−**B**, and Ru−**E**. Similarly, the forming Ru−H′ (Ru−C) bond lengths are shorter, i.e., 1.63 (2.24), 1.62 (2.23), and 1.61 (2.24) Å, respectively. This suggests that the transition structures for Ru−**C**−TS, Ru−**D**−TS, and Ru−**F**−TS take on more productlike character than for the Ru−**A**−TS, Ru−**B**−TS, and Ru−**E**−TS cases. This is in accordance with the greater endothermicity of the former three reactions (see below) than in the case of the latter three systems.

Seventh, our DFT results given in Figures 2−4 show that all the products $Ru(L_3)(H')(CH_3)$ adopt a trigonal-bipyramidal geometry. By examination of those conformations of products, it is obvious that the methane fragment (H′···CH_3) is poised in a σ_{CH_2} fashion, which is consistent with the above findings for the transition states, where the σ_{CH_2} orientation was slightly favored over the π_{CH_2} approach. Thus, the reaction trajectory for C−H insertion suggested by this FMO model (Figure 1) appears to be set in motion in the final product.

IV. Geometries and Energetics of $OsL_3 + CH_4$

The fully optimized geometries of the agostic complex, the transition state, and the product for the insertion of $Os(L_n)(L'_{3-n})$ into the C−H bond of methane are shown in Figures 5−7. Also, their relative energies at the B3LYP/LANL2DZ level are collected in Table 1.

Two points are noteworthy. First, the computational results of the OsL_3 reaction are in principle similar to those noted above for the RuL_3 system in many aspects. Our theoretical investigations suggest that reactants Os−**C**−Rea and Os−**D**−Rea are lower in energy than their corresponding isomers Os−**B**−Rea and Os−**E**−Rea by 13 and 12 kcal/mol, respectively, because of the trans-destabilizing ligands involved, with CO > PH_3.[15] Likewise, the OsL_3 reactants with the triplet ground state would have small excitation energy to the first singlet state as (see Table 1); i.e., $\Delta E_{st} = -3.9 - -3.0$ kcal/mol, implying that the transition from the triplet to the singlet state would be easy because of a large spin−orbit coupling caused by a heavy transition metal.

Second, the B3LYP results also indicate that the σ_{CH_2} orientation for OsL_3 insertion into a saturated C−H bond will be preferred to the π_{CH_2} approach, which will lead to the second-order saddle point. The former transition states were calculated to be 4.7−1.4 kcal/mol lower than the latter transition states as shown in Table 1. When the structure of the transition state for each OsL_3 oxidative addition reaction was checked, it was found that the breaking C−H′ bond lengths of Os−**A**−TS (1.33 Å), Os−**B**−TS (1.39 Å), and Os−**E**−TS (1.49 Å) are in general shorter than those of Os−**C**−TS (1.45 Å), Os−**D**−TS (1.49 Å), and Os−**F**−TS (1.52 Å). Again, the forming Os−H′ (Os−C) bond lengths of the former three structures are 1.72 (2.33), 1.69 (2.31), and 1.67 (2.25) Å, which are longer than those of the latter three structures, i.e., 1.69 (2.30), 1.67 (2.28), and 1.67 (2.29) Å. Thus, these results strongly suggest that Os−**A**−TS, Os−**B**−TS, and Os−**E**−TS should be described as early transition states, whereas Os−**C**−TS, Os−**D**−TS, and Os−**F**−TS are relatively late transition states. As will be shown below, this is in accordance with the larger exothermicity of the former three reactions than in the case of the latter three reactions.

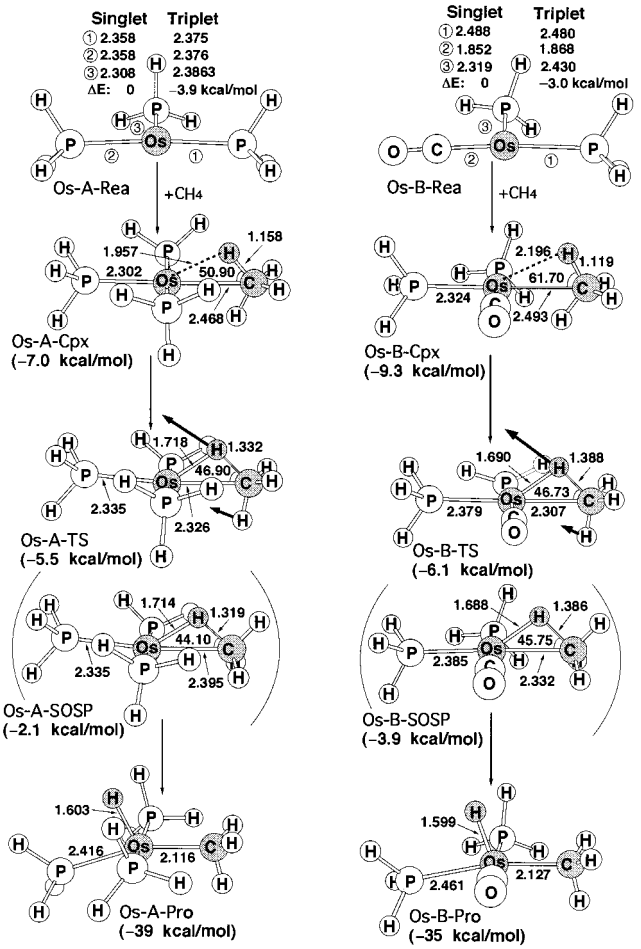

Figure 5. B3LYP/LANL2DZ optimized geometries (in angstroms and degrees) of the reactants (singlet and triplet), precursor complex, transition state, and product of Os−**A** and Os−**B** cases. Values in parentheses are the relative energies at the B3LYP/LANL2DZ level. The heavy arrows indicate the main atomic motions in the transition-state eigenvector.

V. Discussion of the Potential Energy Surfaces

The potential energy profiles based on the data in Table 1 are summarized in Figure 8. Three interesting conclusions can be drawn from this figure.

First, it is apparent that the PH_3 ligand, which is trans to the incoming methane, can enhance the C−H oxidative addition reactions. In particular, for the same metal center, complexes containing more electron-releasing alkylphosphines are considerably more reactive. Namely, this may lead to a lower activation energy and a larger exothermicity for the oxidative addition of H−CH_3 compared to 14-electron T-shaped ML_3 complexes (left to right in Figure 8). For instance, as demonstrated in Table 1, the barrier height for H−CH_3 activation with M = Ru increases in the order Ru−**A** (−1.6 kcal/mol) < Ru−**B** (1.8 kcal/mol) < Ru−**E** (5.7 kcal/mol) < Ru−**C** (9.3

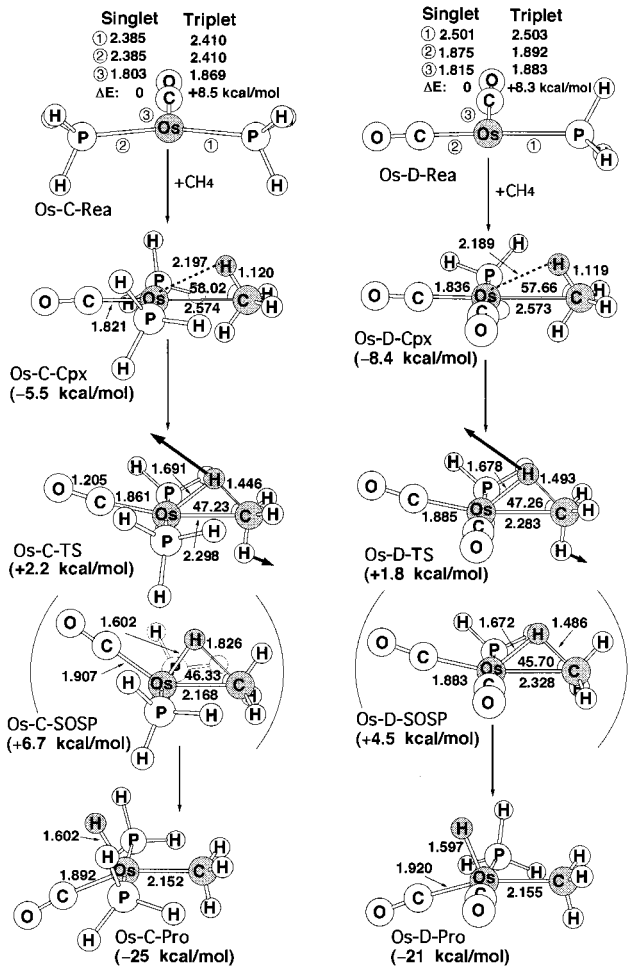

Figure 6. B3LYP/LANL2DZ optimized geometries (in angstroms and degrees) of the reactants (singlet and triplet), precursor complex, transition state, and product of Os−**C** and Os−**D** cases. Values in parentheses are the relative energies at the B3LYP/LANL2DZ level. The heavy arrows indicate the main atomic motions in the transition-state eigenvector.

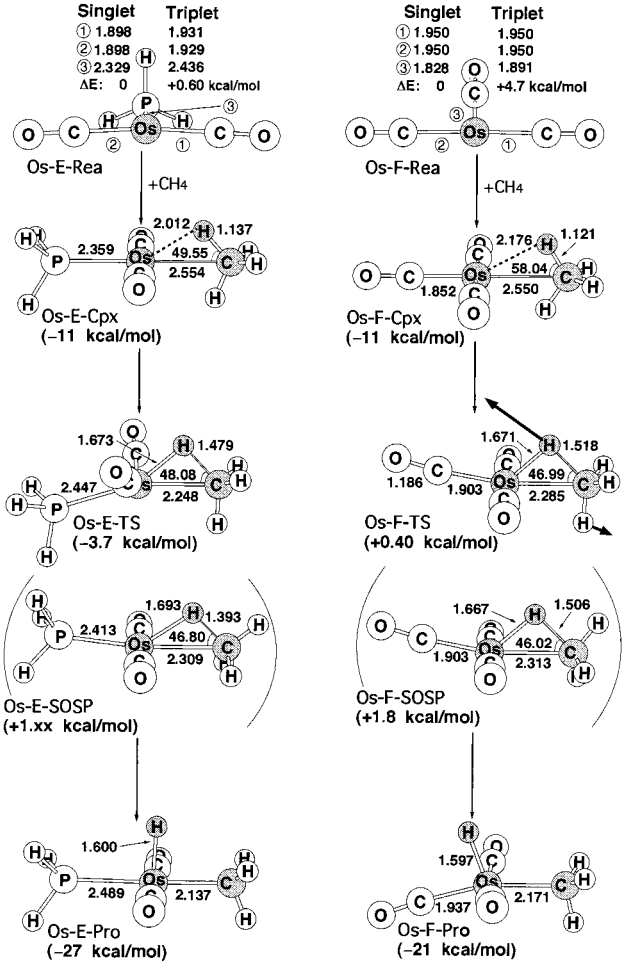

Figure 7. B3LYP/LANL2DZ optimized geometries (in angstroms and degrees) of the reactants (singlet and triplet), precursor complex, transition state, and product of Os−**E** and Os−**F** cases. Values in parentheses are the relative energies at the B3LYP/LANL2DZ level. The heavy arrows indicate the main atomic motions in the transition-state eigenvector.

kcal/mol) < Ru−**D** (11 kcal/mol) ∼ Ru−**F** (11 kcal/mol) and for M = Os, Os−**A** (−6.1 kcal/mol) < Os−**B** (−5.5 kcal/mol) < Os−**E** (−3.7 kcal/mol) < Os−**C** (0.40 kcal/mol) < Os−**D** (1.8 kcal/mol) < Os−**F** (2.2 kcal/mol). Note that the activation barriers for the Os reactions are smaller than those for their Ru analogues.

Second, as seen in Table 1, all the oxidative addition reactions are thermodynamically exothermic. The order of exothermicity follows the same trend as that of the activation energy Ru−**A** (−22 kcal/mol) < Ru−**B** (−15 kcal/mol) < Ru−**E** (−8.7 kcal/mol) < Ru−**C** (−5.2 kcal/mol) < Ru−**D** (−0.91 kcal/mol) < Ru−**F** (−0.74 kcal/mol) and Os−**A** (−39 kcal/mol) < Os−**B** (−35 kcal/mol) < Os−**E** (−27 kcal/mol) < Os−**C** (−25 kcal/mol) < Os−**D** (−21 kcal/mol) ∼ Os−**F** (−21 kcal/mol). Again, the Os reactions are more exothermic than their Ru counterparts.

Third, our model calculations also suggest that oxidative additions involving a third-row transition metal (such as Os) should be preferable to those of a second-row transition metal (such as Ru), since it has been demonstrated not only that the former are thermodynamically more favorable but also that the kinetic barriers associated with them are typically smaller. On the other hand, the reductive elimination (right to left in Figure 8) of the second-row metal is more favorable than that of the third-row homologue. Since there are no relevant experimental and theoretical data on such systems, the above results are predictions.

VI. Origin of the Barrier and Reaction Enthalpy for Oxidative Addition of ML_3

In this section, an interesting model for interpreting the reactivity of oxidative addition reactions is provided by the so-called configuration mixing (CM) model.[17−19] According to the conclusions of this model, the energy barriers governing processes as well as the reaction enthalpies should be proportional to the energy gap ΔE_{st} ($=E_{triplet} - E_{singlet}$) between the singlet and the triplet states of 14-electron ML_3 complexes. In other words, the smaller the ΔE_{st} of ML_3, the lower the barrier height and the larger the exothermicity and, in turn, the faster the oxidative addition reaction.

Our model calculations confirm the above prediction. For the B3LYP/LANL2DZ calculations on the aforementioned six systems, a plot of activation barrier versus ΔE_{st} is given in Figure 9; the best fit is $\Delta E^{\ddagger} = 0.753\Delta E_{st} + 7.10$ and $\Delta E^{\ddagger} = 0.661\Delta E_{st} - 3.44$ for Ru and Os cases, respectively. Likewise, the linear correlations between ΔE_{st} and the reaction enthalpy (ΔH), also obtained at the same level of theory, are $\Delta H = 1.20\Delta E_{st} - 7.49$ and $\Delta H = 1.28\Delta E_{st} - 31.8$, respectively. This

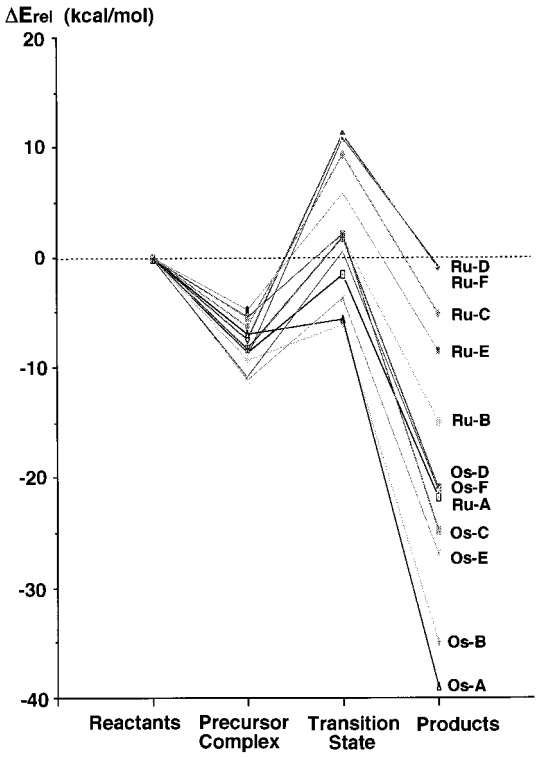

Figure 8. Potential energy surfaces for the activation of H−CH_3 bond by ML_3 (M = Ru, Os; L = PH_3, CO). The relative energies are taken from the B3LYP/LANL2DZ values as given in Table 1. For optimized structures of the stationary points see Figures 2−7.

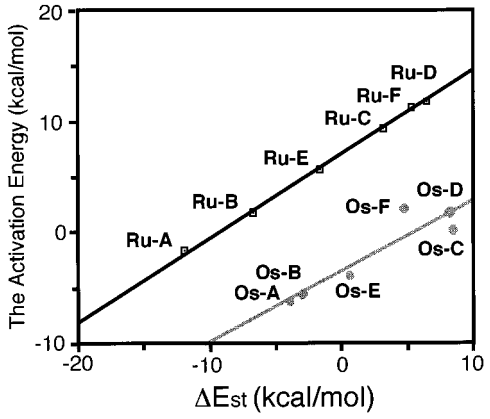

Figure 9. ΔE_{st} ($=E_{triplet} - E_{singlet}$) for ML_3 (M = Ru, Os; L = PH_3, CO) fragments (see the third column in Table 1) vs the activation energy for oxidative addition of ML_3 fragments to H−CH_3 (see the last second column in Table 1). The linear regression equation is $\Delta E^{\ddagger} = 0.756\Delta E_{st} + 7.09$ and is $\Delta E^{\ddagger} = 0.636\Delta E_{st} - 3.45$, with a correlation coefficient $R = 0.998$ and $R = 0.858$, for Ru and Os cases, respectively. All values were calculated at the B3LYP/LANL2DZ level. See the text.

investigation provides strong evidence that the singlet−triplet gap plays a significant role in determining the reactivity of the reactants.

Considering the nature of the central metal, our DFT calculations have shown that oxidative addition to OsL_3 has a lower activation energy than addition to RuL_3. The reason for this can be traced back to the singlet−triplet gap of ML_3. According to the experiments,[20] the Ru atom has a quintet d^7s^1 ground state with a low excitation energy of 19 kcal/mol to the triplet d^7s^1 state. For the Os atom, the ground state is quintet d^6s^2, but with a relatively high excitation energy of 32 kcal/mol to the triplet d^7s^1 state. This implies that Os would prefer to remain in a high-spin state, whereas Ru favors a low-spin state. It is therefore reasonable to conclude that the promotion energy from the singlet state to the triplet state, used to form the strongest covalent bonds, should be smaller for the Os complex than for the Ru complex.

Considering the substituent effect, our theoretical findings suggest that better electron-donating ligands (such as PH_3) give a lower barrier for oxidative addition, while stronger electron-withdrawing ligands (such as CO) give a lower barrier for reductive elimination. In addition, our calculational results have shown that complexes containing more electron-releasing phosphines are considerably more reactive.[21] The reason for these can also be simply understood in terms of the singlet−triplet gap (ΔE_{st}) of the reactants. Qualitatively, since oxidative addition involves charge transfer from the metal center of ML_3 to the incoming methane, a strong electron-donating L, which can increase the electron density on the central metal, would stabilize its transition state and thus lower the barrier height. Furthermore, as mentioned earlier, the PH_3 ligand, which is trans to the incoming methane, can lead to a smaller HOMO($1a_1$)−LUMO($2a_1$) energy difference. This would result in a smaller ΔE_{st} and, in turn, allow a more facile oxidative addition to C−H bonds of alkanes than the ML_3 reactants with a CO ligand trans to the incoming methane.

In summary, with the above analysis on the 14-electron T-shaped *trans*-M(L″)$(L)_2$ (L″ = ligand trans to the incoming methane) reactant in mind, one may then anticipate that a better electron-donor ligand L″ (such as PH_3 and Cl), and a heavier transition metal (i.e., third-row), will lead to a smaller ΔE_{st} and, in turn, will facilitate oxidative addition reactions to saturated C−H bonds. Moreover, the more the electron-donating ligands are attached to the central metal, the more rapid the oxidative addition. Conversely, a complex with a stronger π-accepting ligand L″ (such as CO) and a lighter transition metal (i.e., second-row) will be a good candidate for reductive coupling of C−H bonds. Additionally, the more the electron-withdrawing ligands are attached to the central metal, the faster the reductive elimination.

Acknowledgment. We are very thankful to the National Center for High-Performance Computing of Taiwan and the Computing Center at Tsing Hua University for generous amounts of computing time. We also thank the National Science Council of Taiwan for their financial support.

Appendix: Computational Details

All geometries were fully optimized without imposing any symmetry constraints, although in some instances the resulting structure showed various elements of symmetry. Furthermore, the transition states were characterized by normal-mode analysis to identify them as real transition states (one imaginary frequency) or second-order saddle points (two imaginary frequencies). The DFT calculations used the Becke hybrid functional (B3LYP)[22] as implemented in the Gaussian 94 program.[23]

Effective core potentials (ECP) were used to represent the 28 innermost electrons of ruthenium (up to the 3d shell).[24] Likewise, ECPs were used to represent the 60 innermost electrons of the osmium (up to the 4f shell) atom.[23] For phosphorus and chlorine we also used the Hay and Wadt relativistic ECP.[24] For these atoms, the basis set was that associated with the pseudopotential with a standard LANL2DZ contraction.[23] For hydrogen, carbon, and oxygen atoms the double-ζ basis of Dunning−Huzinaga was used.[26] Moreover, the unrestricted B3LYP approach was used in this work to

describe the triplet states of reactants. Hence, all the B3LYP calculations are denoted by B3LYP/LANL2DZ.[27]

References and Notes

(1) For reviews, see the following. (a) Parshall, G. W. *Acc. Chem. Res.* **1975**, *8*, 113. (b) Bergman, R. G. *Science* **1984**, *223*, 902. (c) Janowicz, A. H.; Perima, R. A.; Buchanan, J, M.; Kovac, C. A.; Struker, J. M.; Wax, M. J.; Bergman, R. G. *Pure Appl. Chem*. **1984**, *56*, 13. (d) Hill, C. L. *Activation and Functionalization of Alkanes*; Wiley: New Tork, 1989. (e) Halpern, J. *Inorg. Chim. Acta* **1985**, *100*, 41. (f) Ephritikhine, M. *New J. Chem*. **1986**, *10*, 9. (g) Jones, W. D.; Feher, F. J. *Acc. Chem. Res.* **1989**, *22*, 91. (h) Ryabov, A. D. *Chem. Rev.* **1990**, *90*, 403. (i) Davies, J. A.; Watson, P. L.; Liebman, J. F.; Greenberg, A. *Selective Hydrocarbon Activation, Principles and Progress*; VCH Publishers. Inc.: New York, 1990. (j) Bergman, R. G. *J. Organomet. Chem*. **1990**, *400*, 273. (k) Koga, N.; Morokuma, K. *Chem. Rev*. **1991**, *91*, 823. (l) Ziegler, T. *Chem. Rev*. **1991**, *91*, 651. (m) Bergman, R. G. *Adv. Chem. Ser*. **1992**, *230*, 211. (n) Wasserman, E. P.; Moore, C. B.; Bergman, R. G. *Science* **1992**, *255*, 315. (o) Crabtree, R. H. *Angew. Chem., Int. Ed. Engl*. **1993**, *32*, 789. (p) Schroder, D.; Schwarz, H. *Angew. Chem., Int. Ed. Engl*. **1995**, *34*, 1937. (q) Lees, A. J.; Purwoko, A. A. *Coord. Chem. Rev*. **1994**, *132*, 155. (r) Amdtsen, B. A.; Bergman, R. G.; Mobley, T. A.; Peterson, T. H. *Acc. Chem. Res*. **1995**, *28*, 154. (s) Ziegler, T. *Can. J. Chem*. **1995**, *73*, 743. (t) Arndtsen, B. A.; Bergman, R. G. *Science* **1995**, *270*, 1970 and references therein. (u) Lohrenz, J. C.; Jacobsen, H. *Angew. Chem., Int. Ed. Engl*. **1996**, *35*, 1305.

(2) For examples of experimental work, see the following. (a) Lian, T.; Bromberg, S. E.; Yang, H.; Proulx, G.; Bergman, R. G.; Harris, C. B. *J. Am. Chem. Soc.* **1996**, *118*, 3769. (b) Bromberg, S. E.; Lian, T.; Bergman, R. G.; Harris, C. B. *J. Am. Chem. Soc.* **1996**, *118*, 2069. (c) Yang, H.; Kotz, K. T.; Asplund, M. C.; Harris, C. B. *J. Am. Chem. Soc*. **1997**, *119*, 9564. (d) Bromberg, S. E.; Yang, H.; Asplund, M. C.; Lian, T.; McNamara, B. K.; Kotz, K. T.; Yeston, J. S.; Wilkens, M.; Frei, H.; Bergman, R. G.; Harris, C. B. *Science* **1997**, *278*, 260.

(3) For examples of theoretical work, see the following. (a) Ziegler, T.; Tschinke, V.; Fan, L.; Becke, A. D. *J. Am. Chem. Soc.* **1989**, *111*, 9177. (b) Song, J.; Hall, M. B. *Organometallics* **1993**, *12*, 3118. (c) Musaev, D. G.; Morokuma, K. *J. Am. Chem. Soc.* **1995**, *117*, 799. (d) Siegbahn, P. E. M. *J. Am. Chem. Soc*. **1996**, *118*, 1487. (e) Su, M.-D.; Chu, S.-Y. *J. Am. Chem. Soc.* **1997**, *119*, 5373.

(4) Gregory, T.; Harper, P.; Shinomoto, R. S.; Deming, M. A.; Flood, T. C. *J. Am. Chem. Soc.* **1988**, *110*, 7915.

(5) For a theoretical study of C−H activation of methane by 14-electron $Rh(Cl)(PH_3)_2$ complex see the following. (a) Koga, N.; Morokuma, K. *J. Phys. Chem.* **1990**, *94*, 5454. (b) Koga, N.; Morokuma, K. *J. Am. Chem. Soc.* **1993**, *115*, 6883. (c) Cundari, T. R. *J. Am. Chem. Soc.* **1994**, *116*, 340. (d) Margl, P.; Ziegler, T.; Blochl, P. E. *J. Am. Chem. Soc*. **1995**, *117*, 12625. (e) Espinosa-Garcia, J.; Corchado, J. C.; Truhlar, D. G. *J. Am. Chem. Soc*. **1997**, *119*, 9891. (f) Su, M.-D.; Chu, S.-Y. *J. Am. Chem. Soc*. **1997**, *119*, 10178.

(6) To reduce the explicit calculations to an easier tractable size within this work, the ancillary ligand $P(CH_3)_3$ has been replaced in all cases by PH_3. The basic results should be unaffected by this simplification.

(7) (a) Bach, R. D.; Andres, J. L.; Su, M.-D.; McDouall, J. J. W. *J. Am. Chem. Soc*. **1993**, *115*, 5768. (b) Bach, R. D.; Su, M.-D.; Aldabagh, E.; Andres, J. L.; Schlegel, H. B. *J. Am. Chem. Soc*. **1993**, *115*, 10237. (c) Bach, R. D.; Su, M.-D. *J. Am. Chem. Soc.* **1994**, *116*, 10103. (d) Su, M.-D.; Chu, S.-Y. *Organometallics* **1997**, *16*, 1621. (e) Su, M.-D.; Chu, S.-Y. *J. Phys. Chem. A* **1997**, *101*, 6798.

(8) Hoffmann, R. *Angew. Chem., Int. Ed. Engl*. **1982**, *21*, 711.

(9) Albright, T. A.; Burdett, J. K.; Whangbo, M. H. *Orbital Interaction in Chemistry*; Wiley: New York, 1985; p 339.

(10) (a) Su, M.-D. *Mol. Phys.* **1993**, *80*, 1223. (b) Su, M.-D. *Mol. Phys.* **1994**, *82*, 567.

(11) (a) Jorgensen, W. L.; Salem, L. *The Organic Chemist's Book of Orbitals*; Academic Press: New York, 1973. (b) Albright, T. A.; Burdett, J. K.; Whangbo, M. H. *Orbital Interaction in Chemistry*; Wiley: New York, 1985; p 138.

(12) In this work, we shall use the σ/π nomenclature (see ref 7) to describe the reaction trajectory and define the axis of attack of the valence orbital on central metal.

(13) Traditionally, the PH_3 ligand is considered as a two-electron σ donor, whereas the CO ligand is considered as a two-electron π acceptor (see ref 9, p 299).

(14) This is due to overlap factors. Recall that there is a smaller atomic orbital coefficient at the center of z^2 than there is in $x^2 - y^2$, and this creates the smaller overlap to the former orbital.

(15) Atwood, J. D. *Inorganic and Organometallic Reaction Mechanisms*; Brooks/Cole Publishing Co.: Monterey, 1985.

(16) (a) Su, M.-D. *Chem. Phys. Lett.* **1995**, *237*, 317. (b) Su, M.-D. *J. Org. Chem.* **1995**, *60*, 6621. (c) Su, M.-D. *J. Phys. Chem*. **1996**, *100*, 4339. (d) Su, M.-D. *Chem. Phys*. **1996**, *205*, 277. (e) Su, M.-D. *J. Org. Chem.* **1996**, *61*, 3080.

(17) (a) Su, M.-D.; Chu, S.-Y. *J. Am. Chem. Soc.* **1997**, *119*, 5373. (b) Su, M.-D.; Chu, S.-Y. *Chem. Phys. Lett.* **1998**, *282*, 25. (c) Su, M.-D.; Chu, S.-Y. *Inorg. Chem.* **1998**, *37*, 3400.

(18) (a) Shaik, S. *J. Am. Chem. Soc.* **1981**, *103*, 3691. (b) Shaik, S.; Schlegel, H. B.; Wolfe, S. *Theoretical Aspects of Physical Organic Chemistry*; John Wiley & Sons Inc.: New York, 1992. (c) Pross, A. *Theoretical and Physical Principles of Organic Reactivity*; John Wiley & Sons Inc.: New York, 1995.

(19) Su, M.-D. *Inorg. Chem.* **1995**, *34*, 3829.

(20) Moore, C. E. *Atomic Energy Levels*; NBS: Washington, DC., 1971; Vol. III.

(21) It has been shown that the use of PMe_3 in place of PH_3 as a model phosphine significantly improves the structural and energetical results. See the following. Clot, E.; Eisenstein, O. *J. Phys. Chem.* **1998**, *102*, 3592.

(22) (a) Becke, A. D. *Phys. Rev. A* **1988**, *38*, 3098. (b) Lee, C.; Yang, W.; Parr, R. G. *Phys. Rev. B* **1988**, *37*, 785. (c) Becke, A. D. *J. Chem. Phys.* **1993**, *98*, 5648.

(23) Frisch, M. J.; Trucks, G. W.; Schlegel, H. B.; Gill, P. M. W.; Johnson, B. G.; Robb, M. A.; Cheeseman, J. R.; Keith, T.; Peterson, G. A.; Montgomery, J. A.; Raghavachari, K.; Al-Laham, M. A.; Zakrzewski, V. G.; Ortiz, J. V.; Foresman, J. B.; Cioslowski, J.; Stefanov, B. B.; Nanayakara, A.; Challacombe, M.; Peng, C. Y.; Ayala, P. Y.; Chen, W.; Wong, M. W.; Andres, J. L.; Replogle, E. S.; Gomperts, R.; Martin, R. L.; Fox, D. J.; Binkley, J. S.; Defrees, D. J.; Baker, J.; Stewart, J. P.; Head-Gordon, M.; Gonzalez, C.; Pople, J. A. *Gaussian 94*, revision B.2; Gaussian, Inc.: Pittsburgh, PA, 1995.

(24) Hay, J. P.; Wadt, W. R. *J. Chem. Phys.* **1985**, *82*, 299.

(25) Hay, J. P.; Wadt, W. R. *J. Chem. Phys.* **1985**, *82*, 284.

(26) Dunning, T. H.; Hay, P. J. *Modern Theoretical Chemistry*; Schaefer, H. F., Ed.; Plenum: New York, 1976; pp 1−28.

(27) It has to be emphasized that calculated DFT barrier heights are often, if anything, too low. See the following. *Chemical Applications of Density Functional Theory*; Laird, A., Ross, R. B., Zeigler, T., Eds.; American Chemical Society, Washington, DC, 1996. Thus, those barrier numbers might be underestimated by down to several kilocalories per mole. It is believed that using the more sphosticipated theory with larger basis sets should be essential. Nevertheless, the energies obtained at the B3LYP/LANL2DZ level can, at least, provide reliably qualitative conclusions.